Polymer Testing 31 (2012) 978–986

Contents lists available at SciVerse ScienceDirect

Polymer Testing

journal homepage: www.elsevier.com/locate/polytest

Property modelling

Influence of prestrain on mechanical properties of highly-filled elastomers: Measurements and modeling

Anders Thorin*, Aurélie Azoug, Andrei Constantinescu

Laboratoire de Mécanique des Solides – CNRS UMR 7649, École Polytechnique, 91128 Palaiseau Cedex, France

ARTICLE INFO

Article history:
Received 5 June 2012
Accepted 23 July 2012

Keywords:
Composite propellants
HTPB
DMA
Prestrain
Generalized Maxwell model

ABSTRACT

The influence of prestrain on viscoelastic properties $|E^*|$ and tan δ of four different HTPB composite propellants was measured using Dynamic Mechanical Analysis (DMA). Nonlinear behaviour in terms of prestrain was observed and then modelled using a modified generalized Maxwell model. Prestrain was introduced as a variable of the stiffness of each Maxwell element using simple two-parameter relationships. An algorithm was proposed and numerically implemented to identify the model parameters from the measurements. The performance of the identification method is discussed in terms of accuracy and robustness. The good match between the predictions and the experimental measurements shows that the dependence on the uniaxial prestrain of the complex modulus of the studied composite propellants can be described with few Maxwell elements but with good accuracy.

1. Introduction

In engineering applications, materials are subject to a complex combination of manufacturing and in-service loadings. Filled elastomers are usually used both in the large strain and small strain regions and their viscous properties play an important role in their structural applications. Therefore, there is an interest in the viscoelastic behaviour of these materials when a static strain is superimposed with an additional fluctuating smaller strain.

This situation has been discussed previously on unfilled rubber in tensile mode [1–4], on carbon black and silica filled elastomers in tensile and shear mode [4–11] and on highly-filled elastomers in torsion mode [12]. In filled elastomers, an increase in storage and loss moduli is observed with increasing prestrain, see for instance [5,8].

A series of experimental observations was recently reported in [4,10] on carbon black-filled rubbers with different filling fraction. The results obtained using a free oscillation technique showed that, at high prestrain levels and for a filler content higher than 50%wt, the storage and loss moduli increase with prestrain. Moreover, the dependence of moduli on prestrain increases with increasing filler fraction. Authors [4,10] explained the increase in loss and storage moduli at large prestrains by considering the molecular orientation of the polymer in combination with the molecular slippage that takes place at the polymer filler interface. The experiments were then extended to measure the influence of the swelling of the materials with various liquids. The storage and loss moduli decrease with increasing degree of swelling. The measured behaviour originates from the decrease in the stiffness of the rubber matrix as well as in the effective volume fraction of the fillers.

In propellants, the filler fraction reaches 80-90% and an important effect of the prestrain is to be expected. In a recent study, Azoug et al. [13] performed an extended experimental campaign in order to understand the role of prestrain for a series of swollen propellant specimens. Nonlinear behaviour exhibiting an increase of both storage and loss moduli is initiated at low prestrain. From the physical point of view, it has been concluded, similarly to

* Corresponding author.
E-mail address: anders.thorin@polytechnique.edu (A. Thorin).

0142-9418/$ – see front matter © 2012 Elsevier Ltd. All rights reserved.
http://dx.doi.org/10.1016/j.polymertesting.2012.07.014

[4,10], that both the swelling of the polymer network and the effective filler fraction drive the viscoelastic response. This nonlinearity depends on the contraction or extension of the polymer chains and could be the result of particle alignment, particularly influential in such highly-filled materials.

The objective of this paper is to propose a simple viscoelastic constitutive law exhibiting the expected behaviour under prestrain, and a fast and robust method to estimate the material parameters from the experimental measurements.

The modelling of the nonlinear viscoelastic mechanical behaviour exhibited by highly-filled elastomers has either been phenomenological [14–16] or obtained through costly computer homogenization techniques [17–21].

Recently, a procedure extending a finite strain viscoelastic model to the frequency domain and taking the prestrain into account has been proposed [22]. The method is based on a linearization in the neighbourhood of the prestrain and on an evaluation of the material behaviour in the frequency-domain. The model was used to characterize carbon black-filled elastomers in [23].

The procedure discussed here was based on a classical generalized Maxwell model. It is shown that introducing a simple dependence of the stiffness on prestrain is sufficient to predict the evolution of storage and loss moduli. The parameters of the model are then identified from experimental measurements by minimising a least squares function. A particularity of the proposed method is the automatic detection of the number of viscoelastic elements necessary to accurately predict the measurements.

2. Materials and experimental characterization

2.1. Materials

The four materials studied here are solid propellants, which are a specific class of highly-filled elastomers. The materials differ in filler fraction, NCO/OH ratio and plasticizer content, as described in Table 1.

The fillers consist of ammonium perchlorate and aluminium particles. The filler fraction varies between 86% wt and 90%wt. The binder is based on hydroxy-terminated polybutadiene (HTPB) prepolymer cured with a methylene diicyclohexyl isocyanate (MDCI). The quantity of MDCI compared to the quantity of polymer introduced corresponds to the NCO/OH ratio, which evolves from 0.8 to 1.1. This reflects the quantity of cross-linking agents available for curing. The plasticizer was dioctyl azelate (DOZ) at between 10%wt and 30%wt of the binder. The materials were thermally cured for 2 weeks at 50 °C.

Table 1
Material composition in terms of filler fraction, NCO/OH ratio and plasticizer fraction.

Material	Filler fraction (%wt)	NCO/OH ratio	Plasticizer (%wt binder)
A	86	0.8	10
B	88	0.8	22.5
C	88	0.95	30
D	90	1.1	10

2.2. Experimental characterization

Dynamic Mechanical Analysis (DMA) was conducted using a Metravib Viscoanalyseur VA3000. Results were interpreted using the algorithms provided by the manufacturer. Dumbbell samples of length 50 mm and section 10 mm × 5 mm were used. The experimental procedure consists in superimposing a tensile prestrain and a sinusoidal strain, which can be expressed as a function of time t as:

$$\varepsilon(t) = \varepsilon_0 + \varepsilon_a \sin(\omega t), \tag{1}$$

where ε_a denotes the strain amplitude, ε_0 denotes the prestrain and ω is the pulsation related to the frequency f through the equation $\omega = 2\pi f$. The tests were performed with a strain amplitude $\varepsilon_a = 0.01\%$ and a frequency $f = 5$ Hz at room temperature. Different levels of prestrain $\varepsilon_{0,i}$ were reached as illustrated in Fig. 1, from 0.01% to about 10%. In one case, failure of the specimen was reached at lower prestrain than 10%.

The complex modulus $|E^*|$ and the loss factor $\tan\delta$ were measured during the DMA experiments. The storage and loss moduli, E' and E'', are deduced from these measurements using equations:

$$E' = |E^*|\cos\delta, \quad E'' = |E^*|\sin\delta, \tag{2}$$

or alternatively:

$$|E^*| = \sqrt{E'^2 + E''^2}, \quad \tan\delta = \frac{E''}{E'}. \tag{3}$$

2.3. Results and discussion

The behaviour of the mechanical parameters $(|E^*|, \tan\delta)$ or equivalently (E', E'') in terms of prestrain dependence exhibits three zones: a linear domain, a transition zone and a nonlinear domain, as shown in Figs. 2 and 3. The linear domain corresponds to the plateau at low prestrain where the viscoelastic properties do not evolve according to prestrain ε_0. The transition phase appears at a prestrain of approximately 1% and a nonlinearity threshold is observed. Finally, the nonlinear domain is the part of the curve where

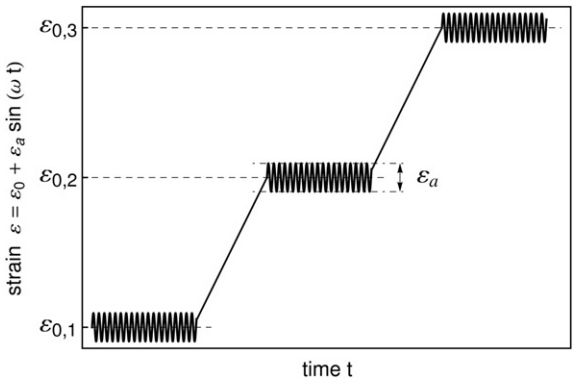

Fig. 1. Schematic representation of the strain history during a prestrained DMA experiment.

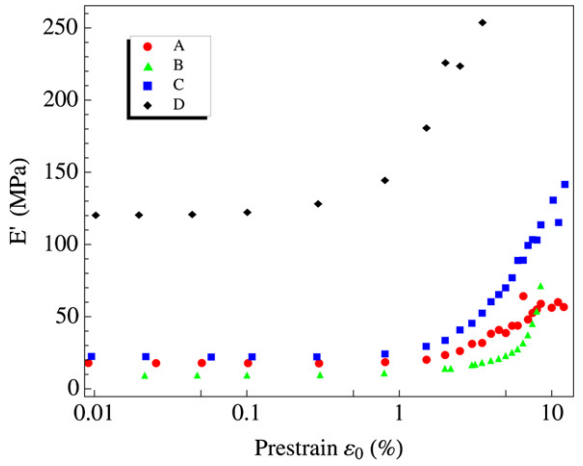

Fig. 2. Comparison of materials A to D, storage modulus E' vs prestrain ε_0, $\varepsilon_a = 0.01\%$.

the viscoelastic properties evolve linearly with the logarithmic prestrain. In the nonlinear domain, storage and loss moduli E' and E'' increase with prestrain ε_0.

A line was fitted on the first four measurements at low prestrain for each material and both moduli. The value at $\varepsilon_0 = 0.01\%$ was chosen to be characteristic of the linear domain. To characterize the nonlinear domain, a line was fitted on the last 6 to 10 measurements and its slope with respect to $\log(\varepsilon_0)$ quantifies the nonlinearity. Finally, the intersection of these lines gives an evaluation of the nonlinear threshold. This rough characterization was used to intercompare the materials. The values obtained are given in Table 2.

Values at low prestrain are similar for material A and C, whereas they are significantly smaller for material B. On the other hand, values for material D are one order of magnitude higher for both moduli, and failure of the sample occurs before a prestrain of 10% could be reached.

These results show that the level of the linear domain in loss and storage moduli increases with filler fraction and

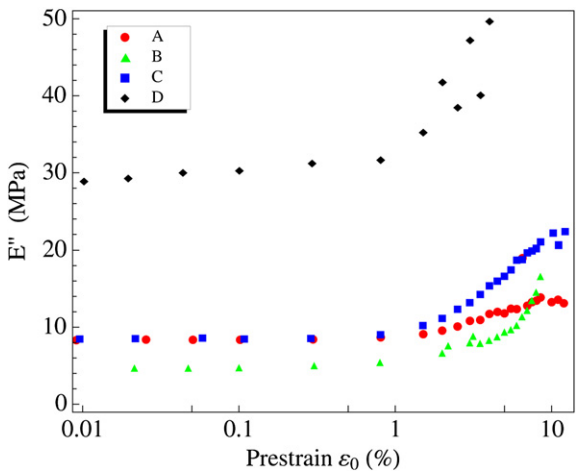

Fig. 3. Comparison of materials A to D, loss modulus E'' vs prestrain ε_0, $\varepsilon_a = 0.01\%$.

Table 2
Values characterizing the linear domain, the transition phase and the nonlinear domain for propellants A to D.

	Linear domain		Thresholds		Slopes	
	E' (MPa)	E'' (MPa)	E' (%)	E'' (%)	E' (MPa)	E'' (MPa)
A	17.4	8.2	1.92	1.22	60.1	6.7
B	9.0	4.6	5.34	4.45	271.4	39.8
C	21.9	8.4	2.28	1.63	152.9	17.2
D	119.6	28.8	0.75	0.39	237.2	22.2

NCO/OH ratio from material A to D (see Table 1), excluding material B. The influence of fillers on the moduli is attributed to the creation of filler-binder bounds in addition to a hydrodynamic effect [24]. On a first order and neglecting more complex interactions at the microscopic scale, the cross-link density increases with the NCO/OH ratio. Therefore, the storage modulus also increases with NCO/OH ratio. Moreover, an increase in NCO/OH ratio also decreases the number of free polymer chains. The free polymer chains are defined as the elastically ineffective chains which are not linked to the network. It is well-known that free polymer chains lead to higher dissipation, and hence undercured elastomers exhibit a high loss modulus [24]. Here, on the contrary, the loss modulus increases with curing. The expected decrease in loss modulus is balanced by the decrease in mesh size resulting from the increase in cross-link density. This decrease in mesh size leads to an increase in friction between polymer chains and in friction between fillers and polymer chains. In addition, the influences of filler fraction and NCO/OH ratio are partially counteracted by plasticizing. Plasticizers reduce the storage modulus by facilitating molecular movements and the loss modulus by decreasing frictions between polymer chains.

Even in the linear domain, material D exhibits extreme behaviour compared to the other materials (Table 2). This material contains more fillers and cross-linking agents, is less plasticized than the others (Table 1) and is, therefore, expected to behave differently. What is remarkable is that the behaviour does not vary linearly with the filler, the cross-linking agent or the plasticizer content. This is a direct consequence of the complexity of the microstructure, i.e. the interactions between the molecules and the fillers at the microscopic scale.

The composition of material B is an optimized combination of average filler fraction, low NCO/OH ratio and relatively high plasticizer content (Table 1). As a consequence, it contains a high fraction of free molecules, either polymer chains or plasticizer. The presence of these molecules explains the low storage modulus value in the linear domain for this material. Moreover, a large mesh size (due to low NCO/OH ratio) and a strong plasticizing effect also tend to decrease the loss modulus value.

The thresholds of the storage and loss moduli are the highest for material B and extremely low for material D. Again, values for materials A and C are similar in spite of their different composition (Table 2).

The initiation of the nonlinearity is commonly associated with the finite extensibility of the network [8–10]. This

material characteristic depends on all the parameters of the composition which influence the structure of the network, including filler fraction, NCO/OH ratio and plasticizer content. Since bounds are created between the fillers and the binder, an increase in filler fraction leads to a decrease in mesh size. The presence of fillers also induces strain amplification [25] which partly explains the low thresholds of material D (Table 2).

Moreover, materials B and C contain the same fraction of fillers and present different thresholds. The main difference between the two propellants is the NCO/OH ratio (Table 1). As the NCO/OH ratio increases, the network cross-link density increases, and hence the thresholds decrease.

Finally, since the thresholds for material A are lower than the ones measured for materials B and C, the influence of fillers on the finite extensibility of the network is counteracted by the influence of plasticizer content. First, plasticizer molecules facilitate movements into the microstructure, and hence increase the network finite extensibility. Second, plasticizers also have an indirect effect on the obtained network. Indeed, these molecules are added to the premix before curing and the material is cured in a swollen state. For a given NCO/OH ratio, adding plasticizers decreases the cross-link density [26].

Slopes of the storage and loss moduli are increasing from materials A to D, except for material B. Material B exhibits the highest slopes (Table 2).

Slopes values increase with increasing filler fraction due to the previously mentioned strain amplification. The microstructure mechanism leading to the measured nonlinearity is also linked to filler-filler interaction [21,26] and, more precisely, to the alignment of filler in the direction of the prestrain.

Additionally, the slopes increase with increasing NCO/OH ratio. Considering the high filler fraction, the local strain is expected to be highly heterogeneous in the binder. Consequently, the network finite extensibility is not uniformly reached at a unique prestrain. The slope is then a quantification of the rate at which the maximally extended part of the network grows with prestrain. Hence, this value depends on NCO/OH ratio as well as filler fraction.

The measured nonlinear behaviour also depends on the single strain amplitude ε_a, as shown in Figs. 4 and 5 for material B. In the linear domain, the storage and loss moduli decrease as ε_a increases. The nonlinearity thresholds are higher and the slopes decrease as the strain amplitude increases.

The decrease of storage and loss moduli with increasing strain amplitude, called the Payne effect, is well-known and specific to filled elastomers [27]. The Payne effect is generally associated with the behaviour of a filler network, which is destroyed and reagglomerated according to strain oscillation at a rate depending on strain amplitude [28]. The existence of a filler network is yet to be proven in highly-filled elastomers such as propellants, since the chemical nature of the non-reinforcing fillers does not necessarily involve a strong attraction between fillers or a strong bound between the fillers surface and the polymeric binder [29,30].

However, since the filler fraction is particularly high, the filler organization into the microstructure has a strong

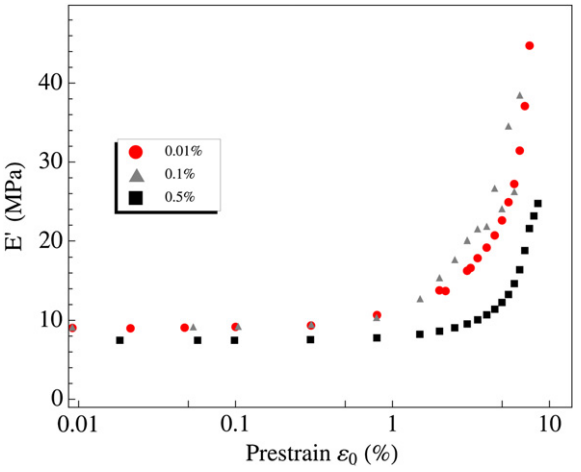

Fig. 4. Influence of strain amplitude ε_a on nonlinearity, material B.

effect on the mechanical behaviour [21]. Hence, high amplitude strain oscillations enable microstructural movements, which relieve internal constraints and lead to a more uniform strain field. This mechanism reduces the strain amplification by the fillers. The prestrain at which part of the network reaches its finite extensibility is then increased while the nonlinearity of the slope decreases.

This experimental study shows that each element of the composition has a strong influence on the nonlinear mechanical behaviour. The interactions between the molecules at the microstructural scale are complex and more tests are required to accurately define and quantify the influences of filler fraction, NCO/OH ratio and plasticizer content. The aim here is to model the behaviour of each of these four materials, which are considered to differ enough to represent the class of highly-filled HTPB-based propellants. The measured nonlinearity is quantitatively dependent on material composition and strain amplitude ε_a but the behaviour is qualitatively identical. This indicates that a model developed for one propellant and one single

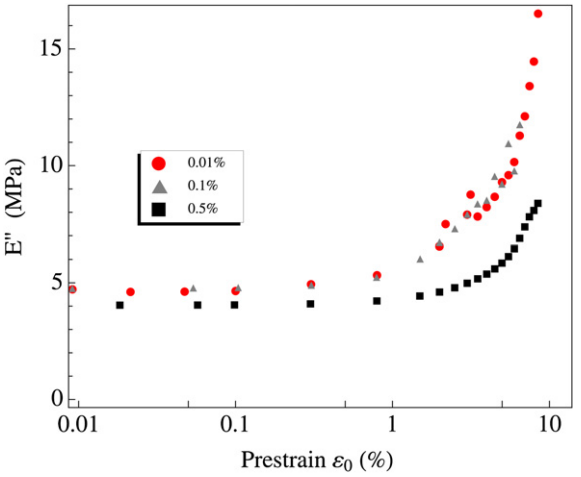

Fig. 5. Influence of strain amplitude ε_a on nonlinearity, material B.

set of experimental conditions could easily be fitted to any other with some quantitative modifications only.

3. Modeling of the nonlinear behaviour

The generalized Maxwell model is often used to model viscoelastic material behaviour [31]. Here, the model was modified under the assumption of small strains to take into account the influence of the prestrain ε_0 on the response measured by $(|E^*|, \tan\delta)$ or equivalently (E',E'').

3.1. Generalized Maxwell model

The generalized Maxwell model and the notations are represented on Fig. 6.

Each viscoelastic element is represented by its stiffness E_i and its viscosity η_i $(i = 1, N)$. The characteristic time of each Maxwell element is defined by: $\tau_i = \eta_i/E_i$. The stress is related to the strain history by the following equation:

$$\sigma(t) = \int_{-\infty}^{t} \left(E_\infty + \sum_{i=1}^{n} E_i e^{-\frac{(t-s)}{\tau_i}} \right) \dot{\varepsilon}(s) ds. \tag{4}$$

The continuous spectrum of relaxation times of the material is described in a generalized Maxwell model by the set of characteristic times $(\tau_1,\ldots,\tau_N)$, which is a priori fixed. The stiffnesses E_i are identified from the experimental data using the further described procedure. E_∞ is fixed and determined from experimental measurements at an extremely low strain rate.

In order to introduce the influence of prestrain on the behaviour, we assume that the stiffness of each viscoelastic Maxwell element is a function of prestrain:

$$E_i = E_i(\varepsilon_0).$$

We shall consider two types of linear dependence of the stiffness with prestrain, either of the form:

$$E_i(\varepsilon_0) = f_i(\varepsilon_0) \quad with \quad f_i(\varepsilon_0) = a_i\varepsilon_0 + b_i$$

or of the form:

$$E_i(\varepsilon_0) = g_i(\varepsilon_0) \quad with \quad g_i(\varepsilon_0) = \begin{cases} 0 & if\ \varepsilon_0 \le c_i \\ a_i(\varepsilon_0 - c_i) & if\ \varepsilon_0 > c_i \end{cases}$$

as illustrated in Fig. 7. The parameters of the two models are grouped in pairs of real positive constants for each branch i: $p_i = (a_i, b_i)$ if $i = 1$ or $i = 2$ and $p_i = (a_i, c_i)$ if $i \ge 3$.

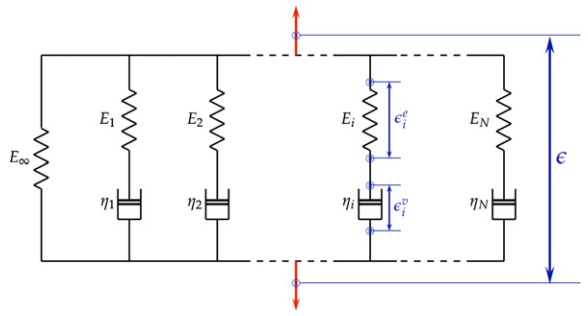

Fig. 6. Generalized Maxwell model with N viscoelastic elements.

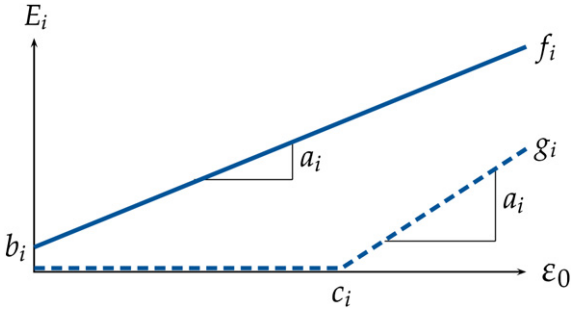

Fig. 7. Dependence of the stiffness E_i of the viscoelastic element i on the prestrain ε_0.

One can note that the element i defined by $E_i = g_i$ has a vanishing stiffness if the prestrain is smaller than c_i, and can be considered to be inactive in the model representation.

As the characteristic times τ_i are a priori fixed, the viscosities η_i evolve with prestrain in order to keep the ratio $\tau_i = \eta_i/E_i$ constant.

The objective is to determine a modified generalized Maxwell model which fits the evolutions of $|E^*|$ and $\tan\delta$ or E' and E'' with prestrain.

3.2. Identification procedure

Let us further assume that a series of measurements of $(|E^*|, \tan\delta)$ is available for K increasing prestrain levels: $\varepsilon_{0_1} < \ldots < \varepsilon_{0_k} < \ldots < \varepsilon_{0_K}$ as displayed in Fig. 1. The identification procedure minimises the cost function J defined in terms of computed and measured complex modulus and loss factor as:

$$J = \frac{\left\| |E^*|^c - |E^*|^m \right\|^2}{\left\| |E^*|^m \right\|^2} + \alpha \frac{\left\| \tan\delta^c - \tan\delta^m \right\|^2}{\left\| \tan\delta^m \right\|^2} \tag{5}$$

where $\cdot^c$ and $\cdot^m$ denote the computed and measured quantities respectively. J is denoted as a cost function in classical optimization theory as the feasible solution minimizes its value. The definitions of $|E^*|$ and $\tan\delta$, Eq. (3), applied to the generalized Maxwell model lead to the following expressions used to calculate $|E^*|^c$ and $\tan\delta^c$ in the cost function:

$$\begin{cases} |E^*|^c = \left[\left(E_\infty + \sum_{i=1}^{n} \frac{(2\pi f\tau_i)^2}{1+(2\pi f\tau_i)^2} E_i \right)^2 + \left(\sum_{i=1}^{n} \frac{2\pi f\tau_i}{1+(2\pi f\tau_i)^2} E_i \right)^2 \right]^{\frac{1}{2}} \\ \tan\delta^c = \left(\sum_{i=1}^{n} \frac{2\pi f\tau_i}{(2\pi f\tau_i)^2} \right) \cdot \left(E_\infty + \sum_{i=1}^{n} \frac{2\pi f\tau_i}{(2\pi f\tau_i)^2} \right)^{-1} \end{cases}$$

The norm $\|\cdot\|$ is the standard vector distance in R^k, where k is the maximum number of prestrain values under consideration. More precisely, the first k measurements of the complex modulus are:

$$|E^*|^m = \left[|E^*|(\varepsilon_{0_1}) \ldots |E^*|(\varepsilon_{0_k}) \right]^T$$

and:

$$\left\| |E^*|^m \right\| = \sqrt{|E^*|(\varepsilon_{0_1})^2 + \ldots + |E^*|(\varepsilon_{0_k})^2}.$$

The real constant α denotes the relative weight between the errors in complex modulus and loss factor. It was chosen equal to 1.

Another possible form for the cost function is obtained by replacing $|E^*|$ and tan δ with E' and E'' in Eq. (5). The conversion between the different pairs of variables is always straightforward using Eq. (2) or (3).

The complete algorithm is described in Fig. 8 and detailed hereafter. It is initialized with two elements (n = 2) of stiffness E_i of the form f_i. In STEP 1, the parameters p_i=(a_i,b_i) are identified starting with $k = 5$ given levels of prestrain and then refined by adding iteratively the next prestrain level.

In STEP 2, the value of the cost function J, defined by Eq. (5), is compared with the acceptable tolerance TOL. If the cost function is higher than the tolerance value, i.e. does not describe the k measurements with enough accuracy, a new Maxwell element $n + 1$ is added to the model and the identification procedure (STEP 1) restarts. Otherwise an additional measurement $k + 1$ corresponding to a higher value of prestrain ε_{k+1} is considered and STEP 1 is started again. The identification procedure continues until it includes all prestrain levels.

The identification algorithm was implemented into Mathematica [32] using standard minimization functions.

4. Results and discussion

The stiffness of the relaxed material E_∞ was measured for material B as 3.31 MPa during complementary testing at extremely low strain rate. The same value was used for all four materials. Updating the value of E_∞ had a small influence on the identification procedure at the strain rates of the DMA experiment. The series of characteristic times τ_i was chosen as 10^{i-3} s, where i is the number of the element.

i) INITIALIZATION:

$n = 2$ viscoelastic elements

$E_i = f_i \quad i = 1, n$

$k = 5$ prestrain levels

ii) STEP 1

Find parameters $\{p_i \mid 1 \leqslant i \leqslant n\}$ by minimizing $\mathcal{J}$

STEP 2: $\mathcal{J} < TOL$?

FALSE

$n = n + 1$

Add new viscoelastic element $E_n = g_n$ with $c_n = \varepsilon_{0_k}$.

GO TO STEP 1

TRUE

IF $k = K$

STOP

ELSE

$k = k + 1$

Add new prestrain ε_{k+1} to the series

GO TO STEP 1

Fig. 8. Algorithm of the identification procedure.

4.1. Identified stiffnesses and output in $|E^*|$, tan δ

The experimental measurements for material B with strain amplitude $\varepsilon_a = 0.01\%$ are shown in Fig. 9, as well as the model responses $|E^*|$ and tan δ identified with the previously described procedure. The corresponding stiffnesses E_i are displayed in Fig. 10, and the corresponding parameters a_i, b_i, c_i are specified in Table 3.

Three different steps of the procedure are represented. The first corresponds to the identification on the first 5 measurements with a prestrain level of up to 0.30%, which requires only the two first Maxwell elements of the model, the tolerance being taken as 0.005. The second step takes into account the first 9 measurements where ε_0 reaches 3.1% and the third element is still not activated ($a_3 = 0$ MPa, $c_3 = 0$). At the final step, $\varepsilon_{0,max} \approx 6.0\%$ and 3 elements are required to describe the measured behaviour on the first 16 measurements, within the given tolerance. With the measurement corresponding to the 17th prestrain level, the cost function value is higher than the tolerance (of 0.005). Therefore, in accordance with the algorithm, a fourth Maxwell element has to be activated.

The response of the identified model can be plotted in terms of (E',E'') using Eq. (2), which is done in the following figures. Fig. 11 shows the experimental measurements as well as the identified model expressed in terms of storage and loss moduli. The relative errors in E' are then 0.35% for the prestrain ε_{0_5}, 1.41% for ε_{0_9}, and 1.97% for $\varepsilon_{0_{16}}$. The relative errors in E'' are 0.32%, 2.67% and 3.94%, respectively. In other words, the identified model applied to material B with $\varepsilon_a = 0.01\%$ and strains up to 6.0% describes the measurements with a relative error of less than 2% in E' and less than 4% in E''.

The corresponding errors in $|E^*|$ and tan δ for $\varepsilon_{0_{16}}$, which is the prestrain of 5.97%, are 1.62% and 2.83%, respectively.

4.2. Identification results in E',E'' for materials A, C, D

The identification procedure was also tested on materials A, C and D and the results are represented in

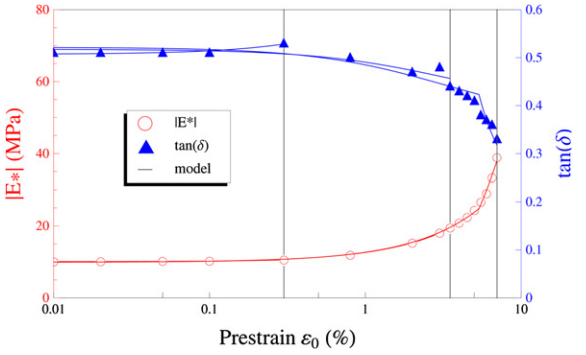

Fig. 9. Model response with stiffnesses of Fig. 10 in $|E^*|$, tan δ, compared with the measurement, material B, $\varepsilon_a = 0.01\%$.

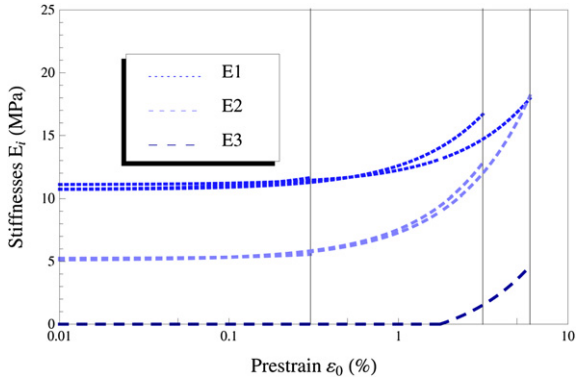

Fig. 10. Identified stiffnesses at three different steps, material B, $\varepsilon_a = 0.01\%$.

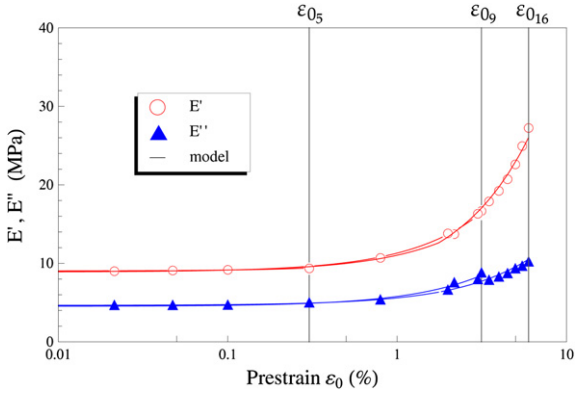

Fig. 11. Model response with stiffnesses of Fig. 10 in $E^{'}$,$E^{''}$, TOL = 0.005.

Figs. 12–14, respectively. The relative errors in $E^{'}$ of the last steps for materials A, C and D are 3.50%, 1.13% and 2.99%, respectively. For the loss modulus $E^{''}$, their values are 1.81%, 2.70% and 27%. The high value of the relative error in $E^{''}$ for material D may be corrected by optimizing in $E^{'}$ and $E^{''}$ instead of $|E^{*}|$ and tan δ or by changing the weighting factor α of the cost function.

The results show that the procedure can generate models which describe the measurements of material A, B, C with $\varepsilon_a = 0.01\%$ up to prestrains of 6% with maximum relative errors of 3.5% in $E^{'}$ and 3.9% in $E^{''}$. One can note that the eighth experimental point of material D breaks the monotony of the curve (cf. Fig. 14). This could be one of the reasons for the greater error in $E^{''}$ for this material.

The identified models present slope discontinuities at prestrains for which Maxwell elements are added. These discontinuities are not physical, they occur at prestrains which correspond to the end of the linear behaviour of the composite and do not break the continuity of the material behaviour.

4.3. Identification results with different ε_a

The algorithm was also used to describe the behaviour of material B with different strain amplitudes ε_a. The results with $\varepsilon_a = 0.01\%$ are shown on Fig. 11. Fig. 15 represents the response of the identified model for $\varepsilon_a = 0.1\%$ and Fig. 16 the response for $\varepsilon_a = 0.5\%$. The relative errors in $E^{'}$ are, respectively, 2.56% and 1.27%, and in $E^{''}$ they are equal to 2.30% and 3.16%. As mentioned previously, for $\varepsilon_a = 0.01\%$ the relative errors in $E^{'}$ and $E^{''}$ are 1.97% and 3.94%, respectively.

4.4. Self-adaptiveness

The procedure automatically activates additional elements when the cost function is higher than the given tolerance. For example, with a tolerance of 0.005 for the measurements of material B and a strain amplitude of $\varepsilon_a = 0.1\%$, the cost function reaches $0.016 > 0.005$ for the model with two elements and the eight first prestrain levels taken into account. The relative error in $E^{'}$ is 3.58%. Therefore, the procedure activates an additional Maxwell element. The new identified parameters of the three elements fit to the measurements with a relative error of 0.36% for the same eight prestrain levels. This illustrates the power of the algorithm, the main obstacle being that the identification does not easily converge with more than three elements. One solution to overcome this difficulty is to switch to an exploratory minimization algorithm. However, a considerable time increase has to be taken into account in such a case.

Finally, the introduction of a new Maxwell element corresponds physically to a change in the behaviour of the composite and is in relation with the phase-divided experimental results.

Table 3
Identified parameters of stiffnesses E_i for material B, plotted on Fig. 10.

ε_0 (%)	a_1 (MPa)	b_1 (MPa)	a_2 (MPa)	b_2 (MPa)	a_3 (MPa)	c_3 (%)
0.30	315.3	10.7	106.5	5.2		
3.14	190.7	10.7	245.6	5.1		
5.97	115.06	11.1	218.6	5.1	110.1	1.76

4.5. Sensitivity to tolerance

The tolerance used in the identification algorithm described in Section 3.2 has to be chosen carefully. In the

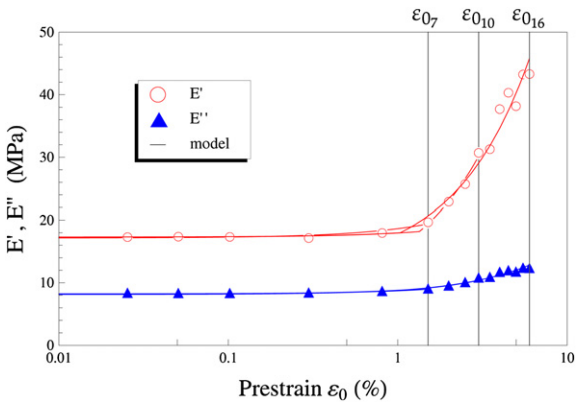

Fig. 12. Response in $E^{'}$,$E^{''}$ of the identified model for material A, $\varepsilon_a = 0.01\%$, TOL = 0.05.

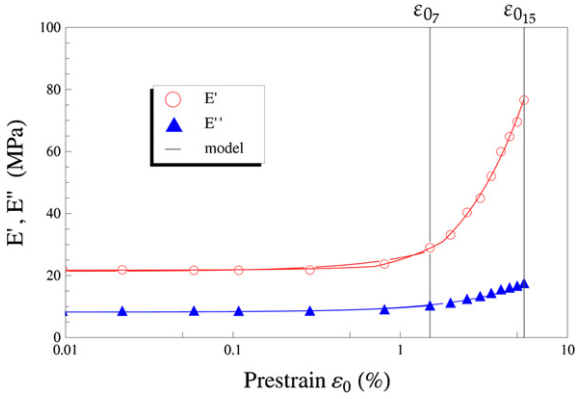

Fig. 13. Response in $E^{'}$,$E^{''}$ of the identified model for material C, $\varepsilon_a = 0.01\%$, TOL = 0.02.

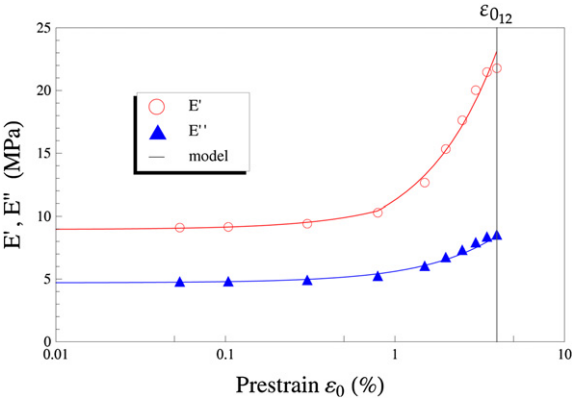

Fig. 15. Response in $E^{'}$,$E^{''}$ of the identified model for material B, $\varepsilon_a = 0.1\%$, TOL = 0.005.

case of noisy measurements, a better match can be obtained by increasing the tolerance. For example, Fig. 12 was obtained with a tolerance of 0.05, whereas Fig. 17 was generated with a tolerance of 0.02. If the tolerance is too low, the algorithm will not be able to fit the noisy measurements accurately enough. When the tolerance is increased, it may produce a description with low relative errors: for material A, 1.99% in $E^{'}$ and 1.22% in $E^{''}$ instead of, respectively, 3.50% and 1.81% for the tolerance of 0.05, but the price to pay for the higher precision is that the identification was done on 12 measurements instead of 16 (cf. Fig. 12).

4.6. Comment

The sensitivity of the results were also tested for other parameters. Increasing or decreasing tenfold E_∞ results in a significant loss of quality and may lead to the non-convergence of the optimization. Similar observations were made for the relaxation times. This necessitates that the values of E_∞ and τ_i are physically realistic. The requirement provides additional proof of the physical consistency of the model.

The series of characteristic times τ_i is a discretization of the continuous memory kernel of viscoelasticity [31] and is supposed to be predefined. The identification of characteristic times translates to the inversion of a linear problem characterized by a large condition number (ratio between largest and smallest singular value of the matrix to be inverted) and, implicitly, to unstable numerical solutions which makes the identification process more difficult. This can be easily checked on a numerical example for a viscoelastic material.

Nevertheless, when E_∞, τ_i and the tolerance were correctly chosen, the procedure identifies models which fit the experiments with relative errors lower than 3.5% for strains up to 6%, for all materials A, B, C, D and for all three strain amplitudes of material B.

The number of Maxwell elements adapts automatically. The identification procedure only lasts a few seconds on a standard computer (in the present case, an Intel Core I5 2.5 GHz processor with 4 Gb SDRAM DDR2). It may not converge within the described accuracy of the Mathematica algorithm of 6 digits for some elements ($i \geq 4$).

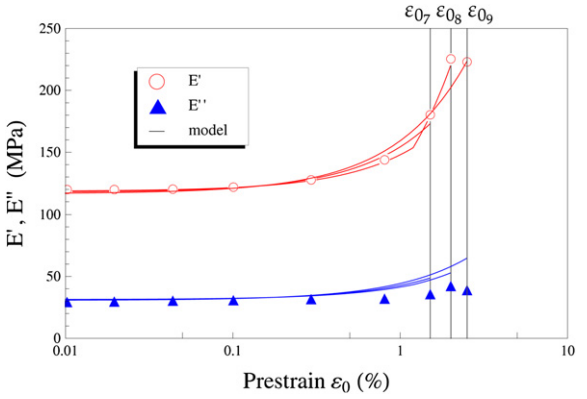

Fig. 14. Response in $E^{'}$,$E^{''}$ of the identified model for material D, $\varepsilon_a = 0.01\%$, TOL = 0.05.

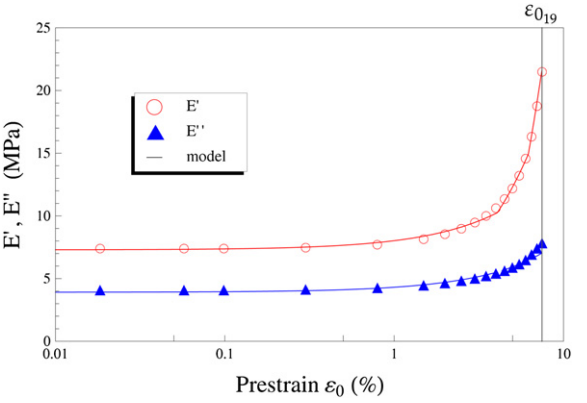

Fig. 16. Response in $E^{'}$,$E^{''}$ of the identified model for material B, $\varepsilon_a = 0.5\%$, TOL = 0.005.

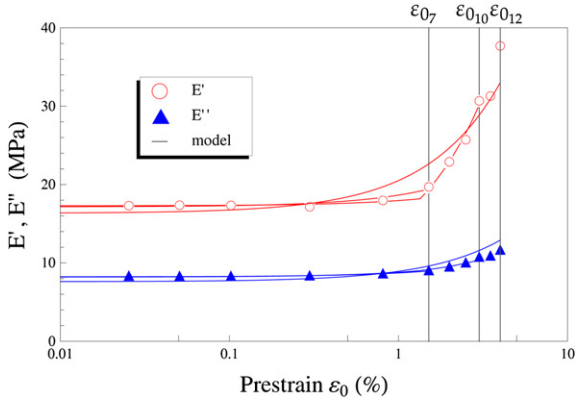

Fig. 17. Response in $E^{'}$,$E^{''}$ of the identified model for material A, tolerance divided by 2.5 compared to Fig. 12, $\varepsilon_a = 0.01\%$, TOL = 0.02.

5. Conclusions

Application of a prestrain superimposed with a small sinusoidal strain produces a nonlinear response in highly-filled elastomers. This nonlinearity was measured and discussed with respect to propellant composition and sinusoidal strain amplitude. The behaviour in both linear and nonlinear domains does not vary linearly with filler, cross-linking agent and plasticizer contents. Alignment of the fillers in the direction of the strain adds to the complex interactions between the molecules at the microscopic scale. A generalized Maxwell model was modified to include the nonlinearity of the material with the applied prestrain. Its relaxation times were fixed and its constant stiffnesses changed to simple functions of two parameters each. An automatic identification procedure was proposed and applied for all four materials and three different prestrain amplitudes. The identified models simulate the experimental observations within a relative error smaller than 3.5% for prestrains up to 6%. For greater prestrains and the same tolerance, new Maxwell elements have to be considered but the algorithm did not manage to converge to the same tolerance.

Acknowledgements

The work of A.A. is financially supported by DGA, Délégation Générale pour l'Armement (France). The authors would like to thank Mrs Amiet (DGA) for supporting this project. The authors particularly thank R. Nevière for his contribution to the experimental work and the many fruitful discussions originating from it.

References

[1] P. Mason, The viscoelastic behavior of rubber in extension, J. Appl. Polym. Sci. 1 (1) (1959) 63–69.
[2] J. Davies, A. Thomas, K. Akutagawa, The effect of low molar mass liquids on the dynamic mechanical properties of elastomers under strain, Progr. Rubber Plast. Technol. 12 (3) (1996) 174–190. 25.
[3] N. Suphadon, A.G. Thomas, J.J.C. Busfield, Viscoelastic behavior of rubber under a complex loading, J. Appl. Polym. Sci. 113 (2009) 693–699.
[4] N. Suphadon, A.G. Thomas, J.J.C. Busfield, The viscoelastic behavior of rubber under a complex loading. II. The effect large strains and the incorporation of carbon black, J. Appl. Polym. Sci. 117 (2010) 1290–1297.
[5] E. Meinecke, S. Maksin, Influence of large static deformation on the dynamic properties of polymers. Part II influence of carbon black loading, Rubber Chem. Technol. 54 (1981) 857–870.
[6] J. Sullivan, V. Demery, The nonlinear viscoelastic behavior of a carbon black-filled elastomer, J. Polym. Sci. Pol. Phys. Ed. 20 (1982) 2083–2101.
[7] K. Arai, J. Ferry, Differential dynamic shear moduli of various carbonblack-filled rubbers subjected to large step shear strains, Rubber Chem. Technol. 59 (1986) 605–614.
[8] A. Voet, J. Morawski, Dynamic mechanical and electrical properties of vulcanizates at elongations up to sample rupture, Rubber Chem. Technol. 47 (1974) 765–777.
[9] N. Dutta, D. Tripathy, Influence of large static deformations on the dynamic mechanical properties of bromobutyl rubber vulcanizates: Part I. Effect of carbon black loading, Polym. Test. 9 (1990) 3–13.
[10] J. Busfield, C. Deeprasertkul, A. Thomas, The effect of liquids on the dynamic properties of carbon black filled natural rubber as a function of prestrain, Polymer 41 (2000) 9219–9225.
[11] R. Warley, D. Feke, I. Manas-Zloczower, Transient effects in dynamic modulus measurement of silicone rubber, Part 2: effect of mean strains and strain history, J. Appl. Polym. Sci. 104 (2007) 2197–2204.
[12] A. Adicoff, A. Lepie, Effect of tensile strain on the use of the WLF equation, J. Appl. Polym. Sci. 14 (1970) 953–966. 26.
[13] A. Azoug, A. Constantinescu, R.-M. Pradeilles-Duval, M.-F. Vallat, R. Nevière, B. Haidar, Effect of the sol fraction and hydrostatic deformation on the viscoelastic behaviour of prestrained highly-filled elastomers, J. Appl. Polym. Sci., in press, http://dx.doi.org/10.1002/app.37800.
[14] S. Ozupek, E. Becker, Constitutive modeling of high-elongation solid propellants, J. Eng. Mater. Technol.-Trans. ASME 114 (1) (1992) 111–115.
[15] S. Ozupek, E. Becker, Constitutive equations for solid propellants, J. Eng. Mater. Technol.-Trans. ASME 119 (1997) 125–132.
[16] G. Ravichandran, C. Liu, Modeling constitutive behavior of particulate composites undergoing damage, Int. J. Solids Struct. 32 (1995) 979–990.
[17] C. Nadot-Martin, H. Trumel, A. Dragon, Morphology-based homogenization for viscoelastic particulate composites. Part I: viscoelasticity sole, Eur. J. Mech. A-Solid 22 (1) (2003) 89–106.
[18] C. Nadot-Martin, A. Dragon, H. Trumel, A. Fanget, Damage modeling framework for viscoelastic particulate composites via a scale transition approach, J. Theor. Appl. Mech. 44 (3) (2006) 553–583.
[19] C. Nadot-Martin, M. Touboul, A. Dragon, A. Fanget, Chapter 12. Direct Scale Transition Approach for Highly-filled Viscohyperelastic Particulate Composites: Computational Study, ISTE/Wiley, 2008, pp. 218–237.
[20] F. Xu, N. Aravas, P. Sofronis, Constitutive modeling of solid propellant materials with evolving microstructural damage, J. Mech. Phys. Solids 56 (2008) 2050–2073.
[21] K. Matous, H. Inglis, X. Gu, D. Rypl, T. Jackson, P. Geubelle, Multiscale modeling of solid propellants: from particle packing to failure, Compos. Sci. Technol. 67 (2007) 1694–1708.
[22] A. Lion, J. Retka, M. Rendek, On the calculation of predeformation-dependent dynamic modulus tensors in finite nonlinear viscoelasticity, Mech. Res. Commun. 36 (2009) 653–658.
[23] P. Höfer, A. Lion, Modelling of frequency- and amplitude-dependent material properties of filler-reinforced rubber, J. Mech. Phys. Solids 57 (2009) 500–520.
[24] A. Medalia, Effect of carbon black on dynamic properties of rubber vulcanizates, Rubber Chem. Technol. 51 (1978) 437–523.
[25] L. Mullins, N. Tobin, Stress softening in rubber vulcanizates. Part I. Use of a strain amplification factor to describe the elastic behavior of filler-reinforced vulcanized rubber, J. Appl. Polym. Sci. 9 (1965) 2993–3009.
[26] A. Azoug, Micromécanismes et comportement macroscopique d'un élastomère fortement chargé, Ph.D. Thesis, Ecole Polytechnique (2010). URL http://tel.archives-ouvertes.fr/tel-00552234/fr/.
[27] A. Payne, The dynamic properties of carbon black-loaded natural rubber vulcanizates. Part I, J. Appl. Polym. Sci. VI (1962) 57–63.
[28] G. Kraus, Mechanical losses in carbon-black-filled rubbers, J. Appl. Polym. Sci.: Appl. Polym. Symp. 39 (1984) 75–92.
[29] R. Stacer, C. Hubner, D. Husband, Binder/filler interaction and the nonlinear behavior of highly-filled elastomers, Rubber Chem. Technol. 63 (1990) 488–502.
[30] R. Stacer, D. Husband, Small deformation viscoelastic response of gum and highly filled elastomers, Rheol. Acta 29 (1990) 152–162.
[31] R. Christensen, Theory of Viscoelasticity: An Introduction, Academic Press, New York, 1971.
[32] 2011wolframresearch inc., mathematica documentation center, http://reference.wolfram.com/mathematica/ref/NMinimize.html.